



# Function of iron-stress-induced protein A in cyanobacterial cells with monomeric and trimeric photosystem I

Parveen Akhtar ,\* Fanny Balog-Vig , Soujanya Kuntam , Szilvia Z. Tóth  and Petar H. Lambrev \*

HUN-REN Biological Research Centre, Szeged, Institute of Plant Biology, Temesvári krt. 62, Szeged 6726, Hungary

\*Author for correspondence: akhtar.parveen@brc.hu (P.A.), lambrev.petar@brc.hu (P.H.L.)

The author responsible for distribution of materials integral to the findings presented in this article in accordance with the policy described in the Instructions for Authors (<https://academic.oup.com/plphys/pages/General-Instructions>) is: Petar H. Lambrev (lambrev.petar@brc.hu).

## Abstract

The acclimation of cyanobacteria to iron deficiency is crucial for their survival in natural environments. In response to iron deficiency, many cyanobacterial species induce the production of a pigment–protein complex called iron-stress-induced protein A (IsiA). IsiA proteins associate with photosystem I (PSI) and can function as light-harvesting antennas or dissipate excess energy. They may also serve as chlorophyll storage during iron limitation. In this study, we examined the functional role of IsiA in cells of *Synechocystis* sp. PCC 6803 grown under iron limitation conditions by measuring the cellular IsiA content and its capability to transfer energy to PSI. We specifically tested the effect of the oligomeric state of PSI by comparing wild-type (WT) *Synechocystis* sp. PCC 6803 with mutants lacking specific subunits of PSI, namely PsaL/PsaI (PSI subunits XI/VIII) and PsaF/PsaJ (PSI subunits III/IX). Time-resolved fluorescence spectroscopy revealed that IsiA formed functional PSI<sub>3</sub>-IsiA<sub>18</sub> super-complexes, wherein IsiA effectively transfers energy to PSI on a timescale of 10 ps at room temperature—measured in isolated complexes and in vivo—confirming the primary role of IsiA as an accessory light-harvesting antenna to PSI. However, a notable fraction (40%) remained unconnected to PSI, supporting the notion of a dual functional role of IsiA. Cells with monomeric PSI under iron deficiency contained, on average, only 3 to 4 IsiA complexes bound to PSI. These results show that IsiA can transfer energy to trimeric and monomeric PSI but to varying degrees and that the acclimatory production of IsiA under iron stress is controlled by its ability to perform its light-harvesting function.

## Introduction

The light reactions of photosynthesis in cyanobacteria are carried out in the thylakoid membranes by the 2 photosystems and the intersystem electron carriers. Light energy is captured by chlorophylls (Chls) and carotenoids in photosystem (PS) I and PSII and by the membrane-associated phycobilisomes (PBS) that transfer the absorbed energy to Chls photosystems. Both the physical association and the energy transfer efficiency between the light-harvesting antenna and the photosystem core complexes can change in response to changes in the environment (Blankenship 2021).

Iron is a particularly important element for cyanobacteria—serving as a cofactor in various metalloenzymes, including

protein complexes involved in respiration, nitrogen fixation, and especially photosynthesis. The photosynthetic apparatus is particularly iron-rich, requiring around 20 iron atoms in the linear electron transport chain (Jia et al. 2021). Therefore, iron deficiency severely hinders photo-induced electron transfer and photosynthetic activity. As iron deficiency is a common nutrient stress in cyanobacterial habitats (Keren et al. 2004), cyanobacteria have evolved a number of diverse acclimation or regulatory strategies to withstand iron deficiency and optimize their photosynthetic performance. Under iron stress, cyanobacterial cells undergo chlorosis (loss of total Chl per cell), reducing the abundance of photosynthetic reaction centers and PBSs content (Öquist 1974; Guikema and Sherman 1983; Chen Bandyopadhyay and

Pakrasi 2018). On the other hand, in response to iron stress, various cyanobacteria species synthesize Chl-binding iron-stress-induced A (IsiA) proteins. IsiA is homologous to PscB—the CP43 core antenna protein of PSII (Bibby, Nield and Barber 2001b; Boekema et al. 2001) and is also known as CP43'. Apart from iron stress, it is also induced and required for growth under other stress conditions, such as high light, salt, heat, and oxidative stress (Vinnemeier Kunert and Hagemann 1998; Singh Li and Sherman 2004; Havaux et al. 2005; Kojima et al. 2006).

IsiA is found in multiple copies that associate in rings around monomeric, trimeric, or tetrameric PSI (Bibby, Nield and Barber 2001a; Boekema et al. 2001). The typical PSI–IsiA supercomplex consists of a closed ring of 18 IsiA around a PSI trimer (Bibby, Nield and Barber 2001a, 2001b; Boekema et al. 2001). Under prolonged iron starvation, IsiA–PSI supercomplexes are formed with different numbers of IsiA and PSI monomers (Yeremenko et al. 2004; Kouřil et al. 2005), including larger ones where PSI is surrounded by double IsiA rings—with 18 IsiA monomers in the inner ring and 25 in the outer—forming a larger IsiA–PSI supercomplex (Chauhan et al. 2011). In addition to associating with PSI trimers, IsiA has been found to form rings and aggregates of its own (Ihalainen et al. 2005; van der Weij-de et al. 2007).

IsiA has been proposed to have a light-harvesting role—as an accessory antenna of PSI (Burnap Troyan and Sherman 1993), as well as a photoprotective one by dissipating excess energy. In iron-starved *Synechocystis* sp. PCC 6803 (*S. 6803*), IsiA can increase the effective absorption cross-section of PSI by 60% (Ryan-Keogh et al. 2012). On the other hand, the accumulation of IsiA aggregates that display much faster excitation decay than other membrane-bound Chl-protein complexes suggests that they serve as a thermal sink (Park et al. 1999; Ihalainen et al. 2005). The mechanism of quenching in IsiA aggregates is not yet determined (Chen et al. 2017). It has also been proposed that IsiA functions as a storage pool for Chls, holding up to 50% of the cellular Chl content during the transition into iron limitation (Singh and Sherman 2007; Schoffman and Keren 2019). During recovery, IsiA provides an accessible reservoir to support the rebuilding of the photosynthetic apparatus.

The structure of a PSI–IsiA complex from *S. 6803* has been determined by cryoelectron microscopy (Toporik et al. 2019). The IsiA monomer resembles CP43 with 6 transmembrane helices but lacks the distinct loop connecting helices V and VI. It coordinates 17 Chls, 13 of which occupy similar positions to CP43 (Toporik et al. 2019) and 4 carotenoids—3 at the IsiA–IsiA interface and 1 between IsiA and PSI. It coordinates Chls-bridging IsiA subunits in the ring and also plays a role in the interaction between IsiA and PSI. Based on a detailed analysis of the X-ray structure of PSI, the PsaF subunit was assigned as a major recognition and interaction site for IsiA (Fromme et al. 2003). It was shown that the lack of PsaF and PsaJ subunits results in the accumulation of smaller, partial IsiA rings (Kouřil et al. 2003). The recent higher

resolution structure confirms that, on the stromal side, the C-terminus of IsiA interacts with PsaF, PsaJ, and PsaK (Toporik et al. 2019).

The capacity of PSI to accept energy from IsiA in the PSI–IsiA supercomplexes depends on the fast photochemical trapping of energy in the PSI core—20 to 50 ps depending on species—and on the energetic coupling between Chls in the IsiA ring and the PSI core. Time-resolved spectroscopy studies of isolated PSI–IsiA complexes from *S. 6803* and *Synechococcus* sp. PCC 7942 have shown that the addition of IsiA increases the trapping time from 20 to 25 ps to 39 to 44 ps (Melkozernov et al. 2003; Andrizhievskaya et al. 2004), which suggests fast and highly efficient energy transfer from IsiA to PSI. However, a wide range of energy transfer times is reported—from under 2 (Melkozernov et al. 2003) to 180 ps at 77 K (Akita et al. 2020). Moreover, these values are based on in vitro studies, but information on the efficiency and dynamics of cyanobacterial energy transfer in vivo is scarce. The variety of PSI–IsiA and IsiA complexes present in thylakoid membranes makes it difficult to evaluate which of its purported roles—light-harvesting, Chl storage, or energy dissipation—is more dominant. Finally, it is not clear how the efficiency of energy transfer depends on the oligomerization state of PSI and the presence or absence of the PsaF/PsaJ subunits.

In this work, we applied steady-state and time-resolved fluorescence spectroscopy to probe IsiA–PSI energy transfer in iron-starved *S. 6803* cells with trimeric PSI (wild-type [WT]), monomeric PSI ( $\Delta$ psaL mutant) and monomeric PSI lacking PsaF and PsaJ subunits ( $\Delta$ FIJL mutant). We show that IsiA is capable of transferring energy in vivo to all types of PSI but to a different extent and that the absence of PsaL, and especially PsaF/J subunits, leads to diminished IsiA levels in the cells under iron deficiency, thereby demonstrating IsiA's primary role as an accessory light-harvesting antenna to PSI.

## Results

### Fluorescence emission spectra of iron-starved cells

The main Chl–protein complexes found in the cyanobacterial thylakoid membranes—PSI, PSII, and IsiA show distinct fluorescence emission spectra at 77 K—IsiA has an emission maximum at 686, PSII at 686 and 696 nm, and PSI around 724 nm (Andrizhievskaya et al. 2002). This difference can be used to estimate the relative abundance of IsiA from the 77 K emission spectra of iron-starved cells. A potential drawback of the method is that it is not possible to tell whether IsiA fluorescence changes are caused by alteration of its concentration in the cell or by changes in its fluorescence lifetime or energy transfer efficiency. Nevertheless, a semiquantitative comparison can be made.

The fluorescence emission spectra of control (+Fe) and iron-starved (–Fe) cells of WT and mutant *S. 6803* cells are compared in Fig. 1 (note that all spectra are normalized to

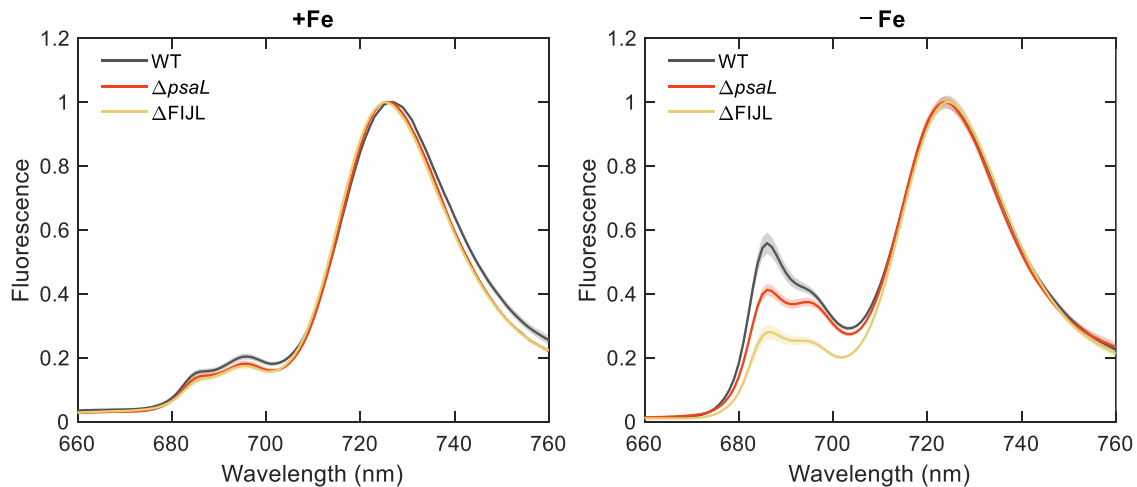


**Figure 1.** Fluorescence emission spectra of intact cells of WT *Synechocystis* sp. PCC 6803,  $\Delta psal$ , and  $\Delta FIJL$  mutants grown in regular BG-11 medium (+Fe) and in a medium devoid of iron (–Fe). The spectra are recorded at 77 K with 440 nm excitation and normalized to the maximum at 724 nm. The +Fe spectra are average of 5, and the –Fe spectra are average of 10 to 13 different batches with SE represented by the shaded area.

the intensity of the PSI emission maximum at 724 nm). The fluorescence spectra of iron-starved cells show the expected increase of emission at 686 nm that corresponds to the accumulation of IsiA (Öquist 1974). However, the 686 nm emission is markedly different in the iron-starved  $\Delta psal$  and  $\Delta FIJL$  mutants compared with the WT, whereas no such differences are present in control (+Fe) cells. Consistent with the fluorescence spectra, the absorption spectra of iron-stressed cells show an increased absorption at 678 nm that is more prominent in WT than in the 2 mutants (Supplemental Fig. S1). From these data, we can hypothesize that the accumulation of IsiA under conditions of iron deficiency depends on the oligomeric state of PSI and the presence of the PsaF subunit.

Based on the fluorescence intensity at 696 nm, we can assess the PSII emission relative to the PSI emission intensity at 724 nm (Table 1). All strains subjected to iron limitation show approximately 2-fold increased PSII:PSI emission ratio compared with the control cells grown in iron-replete medium, which is consistent with a reduced PSI content in the cells. It should be noted, however, that PSII emission in control cells could partly be quenched by spillover (energy transfer to PSI). We estimate that in control conditions, the yield of spillover, i.e. the fraction of excitations created in PSII that are transferred to and trapped by PSI, is about 20% in *S. 6803* cells (Akhtar et al., manuscript under revision). According to Nagao et al. (2021), the IsiA ring around PSI prevents the formation of PSII–PSI megacomplexes and reduces spillover in iron-stressed cells. Therefore, it is reasonable to assume that the increased PSII emission observed in iron-stressed cells is partly because of reduced spillover.

In addition to the increased emission at 696 nm, iron-stressed cells show significantly higher ( $\alpha = 0.01$ , see Materials and Methods) fluorescence intensity at 686 nm, which can be assigned to IsiA emission (Table 1). The estimation is only approximate as it is valid under the assumption

that the 686/696 nm peak intensity ratio is the same in both –Fe and +Fe conditions but, nonetheless, allows us to compare the relative emission from IsiA in the PSI mutants. Both strains with monomeric PSI showed lower IsiA emission relative to the IsiA emission in WT cells—49% and 37% for  $\Delta psal$  and  $\Delta FIJL$ , respectively (with an SE of 12%). The result suggests that the mutants have relatively lower IsiA content.

The fluorescence spectra recorded with 580 nm excitation allow us to compare the PBSS emission in the control and iron-starved cells (Supplemental Fig. S2). In control BG-11 medium, the monomeric mutants show reduced emission at 640 to 650 nm that is consistent with the lower absorption in this wavelength range (Supplemental Fig. S1) and indicates lower abundance of PC in the mutants, as was reported earlier (Akhtar et al. 2022). On the other hand, the mutants have stronger PSII emissions than the WT. Iron-starved cells of both mutant strains show similar differences in the PC wavelength region. In contrast, both  $\Delta psal$  and  $\Delta FIJL$  show lower emissions in the PSII/IsiA region than WT. This result is also consistent with lower IsiA accumulation in the  $\Delta psal$  and  $\Delta FIJL$  strains.

Because intact cells may be prone to artifacts from light scattering and reabsorption of the emitted fluorescence, we have performed the same experiments with isolated thylakoids from control and iron-starved cells. The fluorescence emission spectra were very similar to their counterparts from intact cells (Supplemental Fig. S3 and Table S1) and from the fluorescence intensities at 686 and 696 nm, we estimated approximately the same relative IsiA emission in the mutant thylakoids (49% and 37% for  $\Delta psal$  and  $\Delta FIJL$  relative to IsiA emission in WT thylakoids, SE 10%).

These data strongly suggest that the IsiA content in iron-stressed *S. 6803* cells depends on the oligomerization state of PSI and further on the presence of the PsaF/J subunits. However, it should be noted that the relative fluorescence

**Table 1.** Peak analysis of the 77 K emission spectra of *S. 6803* cells

Strain	Iron	$F_{686}^a$	$F_{696}^a$	$F_{PSII}^b$	$F_{IsiA}^c$
WT	+Fe	12 ± 1 <sup>a</sup>	17 ± 1	12 ± 1	
	−Fe	57 ± 4 <sup>b</sup>	40 ± 2	29 ± 2	28 ± 5
$\Delta psal$	+Fe	13 ± 1 <sup>a</sup>	17 ± 1	13 ± 1	
	−Fe	41 ± 2 <sup>c</sup>	37 ± 2	28 ± 1	14 ± 3
$\Delta FIJL$	+Fe	11 ± 1 <sup>a</sup>	15 ± 1	11 ± 1	
	−Fe	28 ± 3 <sup>c</sup>	25 ± 1	18 ± 1	10 ± 3

<sup>a</sup>  $F_{686}$  and  $F_{696}$  represent the fluorescence intensities (mean ± SE,  $n = 10$  to 13) at 686 and 696 nm relative to the maximal fluorescence around 724 nm (100%). The fluorescence was recorded with 440 nm excitation wavelength. Superscript italic letters a–c denote groups with significant differences of the mean values based on analysis-of-variance.

<sup>b</sup>  $F_{PSII} = F_{696} \cdot \left( \frac{F_{686}}{F_{696}} \right)_{+Fe}$  estimates the PSII emission at 686 nm.

<sup>c</sup>  $F_{IsiA} = F_{686} - F_{PSII}$  estimates the IsiA emission at 686 nm.

intensities cannot be generally equated with the concentrations of IsiA in the cells.

### Circular dichroism spectra of thylakoid membranes and PSI–IsiA complexes

As an additional probe for the changes in the abundance of IsiA, we compared the circular dichroism (CD) spectra of isolated PSI–IsiA complexes and of thylakoid membranes isolated from iron-stressed cells (Fig. 2; Supplemental Fig. S4). The thylakoid membranes were solubilized with detergent to suppress the light scattering. IsiA shows a negative amplitude CD band at 438 nm. In contrast, thylakoids from cells grown in control BG-11 medium have near-zero CD signal at 438 nm and no local minimum in this wavelength range, which makes the 438 nm band a convenient indicator for IsiA.

In line with the fluorescence emission data, we find that the IsiA CD peak is significantly diminished ( $\alpha = 0.01$ ) in the monomeric PSI mutants. The mutants also show CD changes in the UV region, which are of unknown origin. We take the differential CD amplitude at 448 and 438 nm as representative of IsiA (as it is negligible in control thylakoids). Considering that the CD signal is proportional to the respective chromophore concentration, it can be estimated that thylakoids of  $\Delta psal$  and  $\Delta FIJL$  contain, respectively, 57% ± 8% and 48% ± 9% IsiA as compared with WT.

### Immunoblotting quantification

As a further test for the IsiA content of iron-starved *S. 6803*, we performed immunoblotting analysis with antibodies against IsiA and the PsaA subunit of PSI (Fig. 3). As expected, in iron-deficiency conditions IsiA accumulated in WT cells at the expense of photosystems (PsaA). Both the  $\Delta psal$  and  $\Delta FIJL$  mutants showed lower relative IsiA content and higher PSI content than the WT. On a total Chl basis, the estimated IsiA content was 58% and 45% for  $\Delta psal$  and  $\Delta FIJL$  compared with WT—in excellent agreement with the CD spectroscopy results.

### Fluorescence kinetics of PSI–IsiA

The steady-state spectroscopy data show that the concentration of IsiA in iron-stressed *S. 6803* is affected by PSI abundance. Next, we performed time-resolved fluorescence spectroscopy

measurements to probe the efficiency of energy transfer in the intact cells. More specifically, we aimed to determine the dynamics of energy transfer from IsiA to PSI in the intact cells and whether IsiA can effectively function as a light-harvesting antenna of PSI in the absence of the PsaL and PsaF subunits.

The fluorescence kinetics of cells were measured at room temperature in the range of 610 to 744 nm and of isolated complexes in the range of 670 to 744 nm with 440 nm excitation wavelength, which excites predominantly Chl. Global multiexponential analysis of the fluorescence decays was applied to obtain fluorescence decay lifetimes and decay-associated emission spectra (DAES). The fluorescence kinetics of isolated IsiA and PSI–IsiA complexes can be described with 3 DAES (Fig. 4). IsiA fluorescence decays with lifetimes of 70 ps, 0.5 ns, and 2.5 ns. The shorter lived component shows the well-known fluorescence quenching of IsiA aggregates (Ihalainen et al. 2005), whereas the longer lived components may originate from monomeric IsiA, as evidenced by the blue-shifted DAES.

The fluorescence of PSI–IsiA complexes decays with a main lifetime of 42 ps. The 2 longer lived components with lifetimes of 272 ps and 3 ns likely represent uncoupled IsiA complexes and Chls. The total trapping time of PSI–IsiA (42 ps) is markedly and significantly ( $\alpha = 0.01$ ) longer than that of isolated PSI alone (26 ps, see Supplemental Fig. S5), evidently due to energy migration between IsiA and PSI. We can roughly estimate the energy migration time  $\tau_{mig}$  by considering the relationship  $\tau_{tot} = \tau_{tr} + \tau_{mig}$ , where  $\tau_{tr}$  is the trapping time of PSI alone and  $\tau_{tot}$  is the total decay time of PSI–IsiA. It follows that the IsiA–PSI energy transfer time in these complexes is approximately 16 ps, in good agreement with published results (Melkozernov et al. 2003; Andrizhiyevskaya et al. 2004; Chauhan et al. 2011). Note that the effective migration or equilibration time depends not only on the size of the IsiA antenna but also on the excitation conditions—in these experiments, we can estimate that the excitation pulses with 440 nm wavelength should excite approximately equally PSI and IsiA in PSI<sub>3</sub>–IsiA<sub>18</sub> complexes.

Figure 5 compares the DAES for the fluorescence kinetics measured from control and iron-starved cells. The fluorescence kinetics of control cells (+Fe) can be described with 3 decay lifetimes, plus an additional ns component with negligible amplitude. The fastest-decaying component with a lifetime of ~25 ps belongs almost exclusively to PSI (Gobets and van Grondelle 2001; Akhtar et al. 2021). A small contribution from PBS is visible in the wavelength region below 660 nm, where a negative peak signifies excitation equilibration (energy transfer) within the PBSs, typically observed on this timescale (Tian et al. 2012; Akhtar et al. 2020). The 2 slower-decaying components with lifetimes of 170 and 550 ps (in WT) show the decay of PSII and partially PBS fluorescence. In comparison with the control, the amplitudes of the 2 long-lived components increase 3-fold in iron-stressed cells, which can be attributed to emission from IsiA complexes. Moreover, the short-lived decay components (35 to 42 ps) have lifetimes and DAES that are similar to that of PSI–IsiA supercomplexes. Similar results in terms of

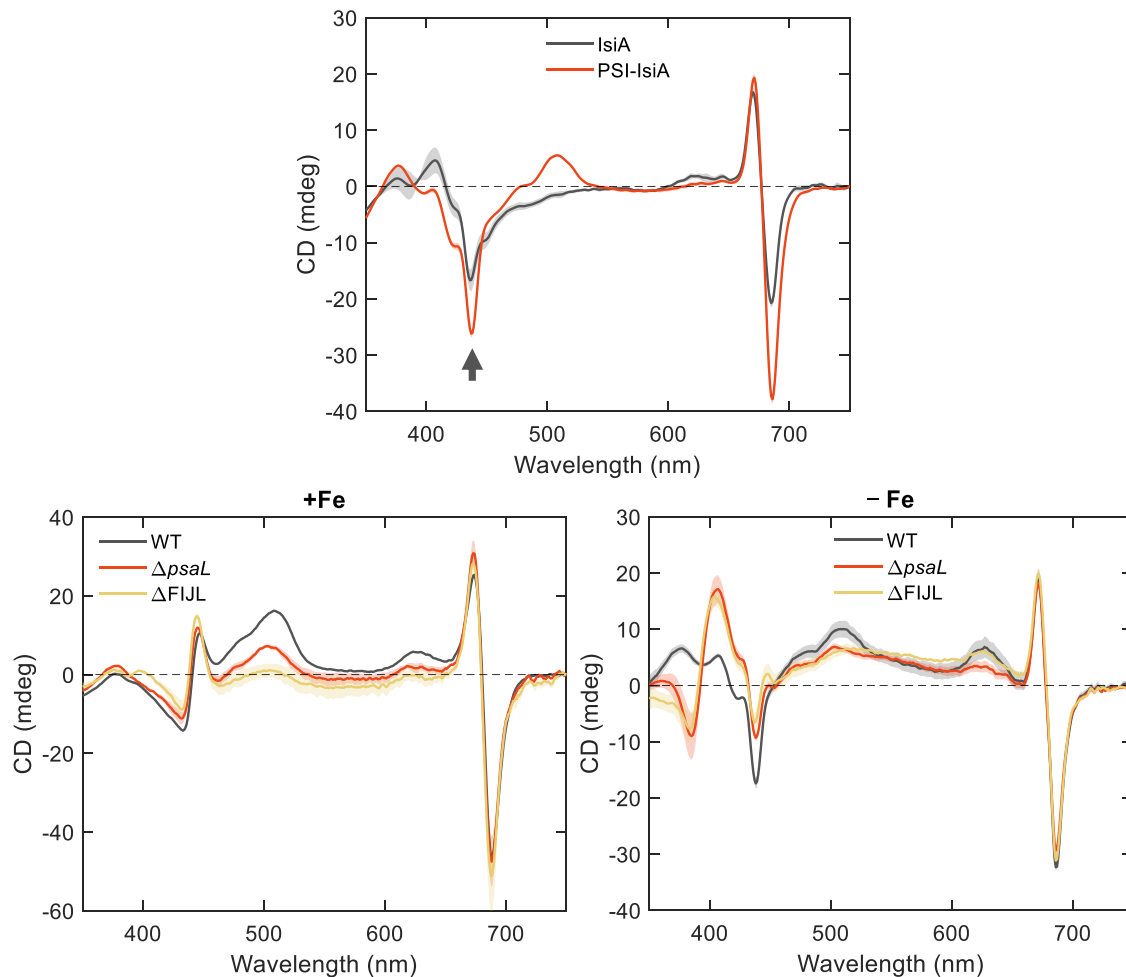


**Figure 2.** Room-temperature CD spectra of IsiA and PSI–IsiA complexes isolated from WT *S. 6803* and of thylakoid membranes of control (+Fe) and iron-stressed (–Fe) *S. 6803* WT,  $\Delta psal$ , and  $\Delta FIJL$ , measured in buffer containing 0.03%  $\beta$ -DM. The spectra are normalized to unity absorbance at the Chl  $Q_y$  maximum. The arrows indicate the IsiA-specific CD band at 438 nm. The figures show average spectra from 3 to 4 independent measurements on different batches with ses represented by the shaded area.

fluorescence lifetimes and DAES features were obtained from thylakoid membranes isolated from control and iron-starved cells (Supplemental Fig. S6).

We ascribe the 35 to 42 ps DAES to PSI–IsiA supercomplexes (cf. Fig. 4) and the longer-lived decay components to energetically decoupled IsiA (and partially to PSII emission). Decay lifetimes in the 70 to 100 ps range are not resolved in intact cells, which may suggest that isolated IsiA aggregates are more strongly quenched than IsiA in the cells. The longer-lived components ( $\sim 170$  and 600 ps) in –Fe conditions, similarly to control cells, show sizeable amplitudes below 660 nm that can be ascribed to emission from PSII equilibrated with PBS. In contrast, isolated IsiA and PSI–IsiA complexes emit virtually no fluorescence in this wavelength range (Supplemental Fig. S7).

From the above, we conclude that the iron-stressed cells of *S. 6803* contain both PSI–IsiA supercomplexes and unconnected IsiA aggregates. The same applies to the 2 mutants. It is noticeable that the relative amplitudes of the long-lived DAES associated with free IsiA are lower in the mutants, in line with the

overall lower emission and concentration of IsiA in these cells. For instance, the wavelength-integrated amplitude of the 170 ps IsiA component relative to the 40 ps PSI component is reduced by 30% in  $\Delta FIJL$  compared with the WT (Supplemental Table S2). The PSI–IsiA lifetime is also slightly shorter in the mutants, especially in  $\Delta FIJL$ —35 ps compared with 42 ps in WT. From the difference between the PSI lifetimes in control cells and the PSI–IsiA lifetimes in iron-starved cells, we estimate that the migration time in WT cells is about 15 ps—almost equal to that of the isolated PSI–IsiA complexes from the same strain, whereas for  $\Delta psal$  and  $\Delta FIJL$ , it is 10 ps. The shorter apparent migration time may indicate that PSI monomers that lack the PsaF subunit connect fewer IsiA units than PSI monomers with the PsaF subunit present.

### Quantification of IsiA from time-resolved fluorescence

To estimate the fractions of IsiA complexes connected to PSI and free IsiA aggregates, we apply a kinetic model fitting to

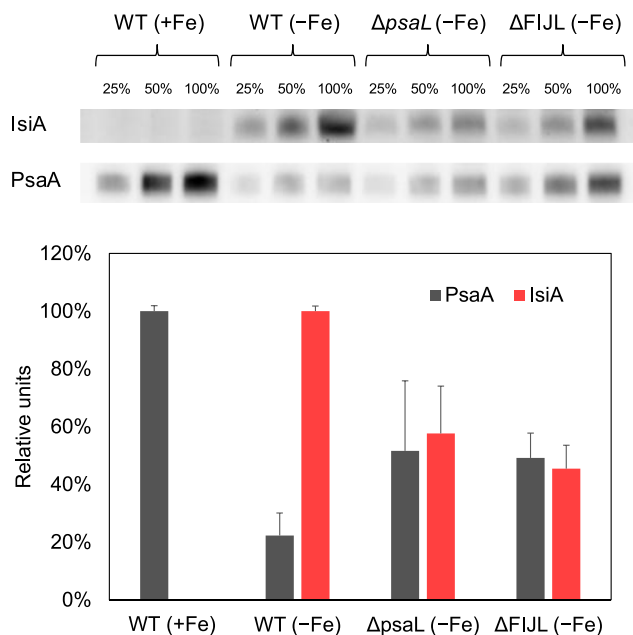


**Figure 3.** Immunoblotting analysis of PSI and IsiA content. Top—representative immunoblots to monitor the changes in IsiA and PsaA (PSI subunit A) levels in thylakoid membranes isolated from control *S. 6803* WT cells grown in regular BG-11 medium (+Fe) and from WT,  $\Delta psal$ , and  $\Delta FIJL$  cell cultures grown in iron-deficient medium (–Fe). Each gel lane was loaded with 0.025, 0.05, or 0.1  $\mu\text{g}$  Chl (100%). The faint background in the IsiA bands of control (+Fe) samples is probably due to reactivity of the IsiA antibodies with PSII (CP43). Bottom—averaged PsaA and IsiA concentrations (relative to WT) estimated from densitometric analysis of immunoblots. SEs from 3 replicates are indicated. Densitometric analysis was done using GelAnalyzer 19.1 ([www.gelanalyzer.com](http://www.gelanalyzer.com)) by Istvan Lazar Jr., PhD, and Istvan Lazar Sr., PhD, CSC.

the DAES. The average number of IsiA in the PSI–IsiA complexes determines the effective trapping lifetime and the shape of the PSI–IsiA DAES—more IsiA complexes result in stronger emission from IsiA and a longer trapping lifetime and vice versa. Unconnected IsiA complexes mainly contribute to the amplitude of the longer-lifetime components (170 and 600 ps). Following this, the sizes of both IsiA pools can be found by a simple fit, as illustrated in Fig. 6 and Supplemental Fig. S8 (for more details, see Supplemental Method S1). Briefly, we model a pool of IsiA connected to PSI through reversible energy transfer. The size of this pool determines the shape and lifetime of the PSI–IsiA DAES. The PSI–IsiA complex in the model has an average decay lifetime of  $\sim 40$  ps with approximately equal excitation of both compartments, whereas the trapping time of PSI alone would be 25 ps. Therefore, the effective equilibration time is  $\sim 15$  ps. The 2 unconnected compartments represent free IsiA and PSII that are quantified from the amplitudes of the respective DAES.

The results of the quantification are summarized in Table 2 for the 3 *S. 6803* strains. The analysis reveals that the relative PSI content (per Chl basis) of the monomeric strains is higher than the WT, whereas the relative IsiA content is lower—in

agreement with the immunoblotting analysis (Fig. 3). Furthermore, we estimate 6 to 7 IsiA complexes connected to PSI in WT cells, which is consistent with 18 IsiA per PSI trimer (Kouřil et al. 2003). Note that the model was validated on isolated PSI–IsiA complexes, for which the fitting yielded an IsiA:PSI molar ratio of 6:1, consistent with the known structure (Toporik et al. 2019). In WT cells, we find an additional 4 to 5 unconnected IsiA per PSI monomer to a total IsiA:PSI molar ratio of about 11:1. This value is in close agreement with the results of Fraser et al. (2013), who estimated a molar IsiA:PSI ratio of 12 in *S. 6803* grown under similar iron-limited conditions. In the monomeric PSI strains, we find that both the connected and unconnected IsiA pools are reduced compared with WT cells. The total IsiA:PSI molar ratios were 58% and 38% for  $\Delta psal$  and  $\Delta FIJL$  cells, respectively. The PSI subunit knockouts appeared to affect both the connected and the free IsiA pools to a similar extent.

### Low-temperature fluorescence kinetics

The fluorescence kinetics of *S. 6803* cells grown in control and iron-deficient media were recorded at a temperature of 77 K with 440 nm excitation (Fig. 7). The DAES of the control cells essentially reproduce previously published results with isolated thylakoids (Akhtar et al. 2021).

The kinetics of control iron-replete cells can be represented with 4 decay lifetime components (plus an additional lifetime in the nanosecond range of very low amplitude that will be omitted from the analysis). The shortest-lived component signifies energy transfer from the bulk antenna Chls to the long-wavelength forms in PSI, concomitant with trapping bulk excitations in the reaction center with an effective time-scale of  $\sim 20$  ps. Faster energy transfer components have been shown in isolated thylakoid membranes that are not resolved in the present analysis (Akhtar et al. 2021). The 3 longer-lived components show DAES peaking at approximately 710, 720, and 725 nm and are assigned to different red Chl pools. In accordance with earlier results, the amplitude of the intermediate-energy component with a maximum around 710 nm is lower in both mutants with monomeric PSI,  $\Delta psal$ , and  $\Delta FIJL$  due to the missing red Chls at the monomer interface in the vicinity of the PsaL subunit (Akhtar et al. 2021).

In comparison with control +Fe cells, iron-stressed cells show markedly different DAES at 77 K, especially regarding the faster-decaying components. The first one, with a lifetime of 27 ps, has a positive maximum at 680 nm and a negative one around 715 to 720 nm. In contrast, the positive maximum associated with the bulk PSI antenna in control cells is close to 690 nm. The peak at 680 nm strongly suggests that this component represents energy transfer from IsiA to PSI (in addition to equilibration within PSI). However, the main decay lifetime of IsiA is 80 to 90 ps, and the negative maximum of the corresponding DAES in the far-red region shows that this component represents energy transfer to PSI as well. Thus, IsiA–PSI transfer can be described with 2 lifetimes—around 30 and 80 to 90 ps. This result alone cannot explain

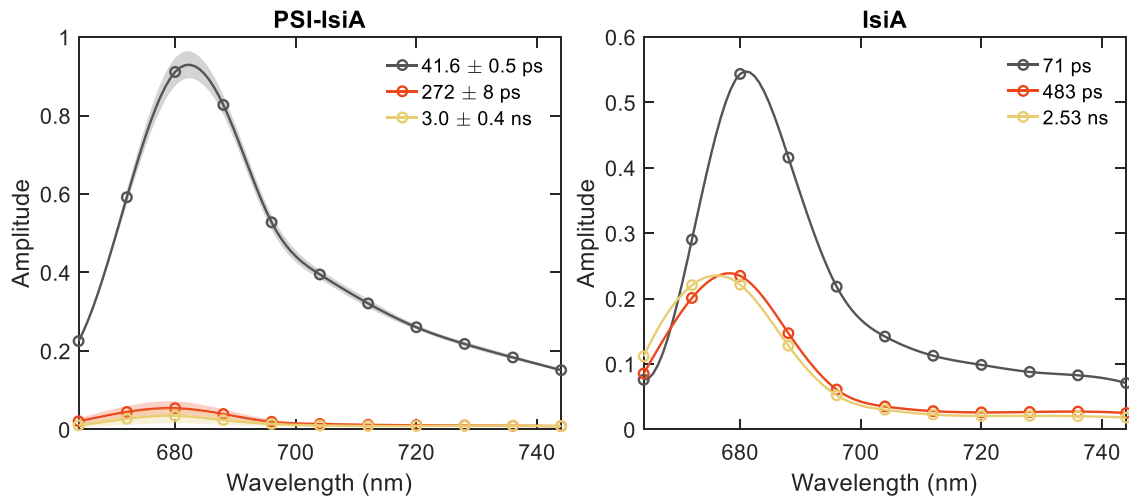


**Figure 4.** Decay-associated emission spectra (DAES) of PSI–IsiA and IsiA complexes isolated from *S. 6803* (WT) cells grown in iron-deficient medium. The spectra are obtained by global lifetime analysis of the fluorescence decays recorded at room temperature with 440 nm excitation. The DAES are scaled so that their sum is equal to one at 680 nm. The spectra of PSI–IsiA are averages of 3 independent replicates. The shaded areas represent se.

the large decrease in the 680 nm fluorescence intensity in the steady-state emission spectra. In addition, we observe non-transferring IsiA that decays with a lifetime of 300 ps.

Qualitatively, both mutant strains with monomeric PSI show similar fluorescence kinetics at 77 K as the WT under iron-deficiency conditions. The amplitudes of the 27 and the 80-ps DAES at 680 nm are lower in the  $\Delta$ FIJL mutant when compared against the amplitudes of the PSI components in the far-red region, which is consistent with the lower number of IsiAs connected to PSI. The amplitude of the 300-ps DAES at 680 nm is also diminished in both mutants but especially in  $\Delta$ FIJL. Thus, the results suggest that the lower fluorescence intensity in the steady-state spectra of the iron-stressed mutants compared with the WT is due to the reduced number of IsiA complexes, both connected to PSI and, to a larger extent, the highly fluorescent nontransferring IsiA.

## Discussion

### Trimeric PSI forms functional supercomplexes with IsiA in vivo

The capability of many species of cyanobacteria to form rings of IsiA (CP43') under iron stress has been known for more than 2 decades (Bibby, Nield and Barber 2001a; Boekema et al. 2001). It is also well established that the IsiA subunits in isolated PSI–IsiA supercomplexes are functionally connected to the PSI core via efficient energy transfer (Melkozernov et al. 2003; Andrizhievskaya et al. 2004; Chauhan et al. 2011). There is no reason to doubt that a similar energetic connectivity also occurs in vivo. The efficient energy transfer allows IsiA to increase the absorption cross-section of PSI, allowing it to trap more photon energy per unit time, in this way reducing the number of Fe-rich PSI complexes necessary to maintain photosynthesis. Nevertheless, several authors have suggested that IsiA has

functions other than to facilitate PSI light harvesting—such as dissipating excess light energy, maintaining PBSs, and storing Chls until more favorable conditions (see Chen Bandyopadhyay and Pakrasi 2018 and references therein).

This study investigates the physiological role of IsiA by evaluating its ability to transfer energy to PSI in intact cells of iron-starved *S. 6803*. To this end, we compare the picosecond Chl fluorescence kinetics of cells and of isolated PSI–IsiA complexes as a reference. The isolated complexes showed that excitations are trapped on a timescale of 42 ps. Similar trapping times were found in PSI–IsiA from *S. 6803* (Melkozernov et al. 2003). From the difference between the trapping time in the supercomplex and the PSI core, it follows that the effective timescale of energy equilibration between IsiA and the PSI core is about 15 to 16 ps, which is close to the 10 ps lifetime of energy transfer determined by transient absorption spectroscopy (Melkozernov et al. 2003).

We found that the PSI kinetics in intact WT *S. 6803* cells subjected to iron deficiency were remarkably similar to that of isolated PSI–IsiA. Not only was the main trapping lifetime identical (42 ps), but the corresponding DAES had virtually identical shapes, that can be approximated as the sum of the PSI core (60%) and IsiA (40%) emission. The similarity strongly suggests that the kinetics of energy transfer in PSI–IsiA in vivo is the same as in an isolated state and that the isolated PSI–IsiA sample is representative of the naturally occurring structural organization. Time-resolved fluorescence spectroscopy of cells at 77 K revealed 2 lifetimes of IsiA–PSI transfer in cells—20 to 30 and 80 to 90 ps. Similar lifetimes were observed in isolated PSI–IsiA at 77 K (Akita et al. 2020). These results further support the functional equivalence of PSI–IsiA complexes isolated in vitro and in the intact thylakoid membrane. Recently, Nagao et al. (2023) published the structure of a supercomplex from *Anabaena* sp. PCC 7120 with monomeric PSI lacking the PsaL subunit and 6 IsiA subunits connected on the PsaA side. Time-resolved

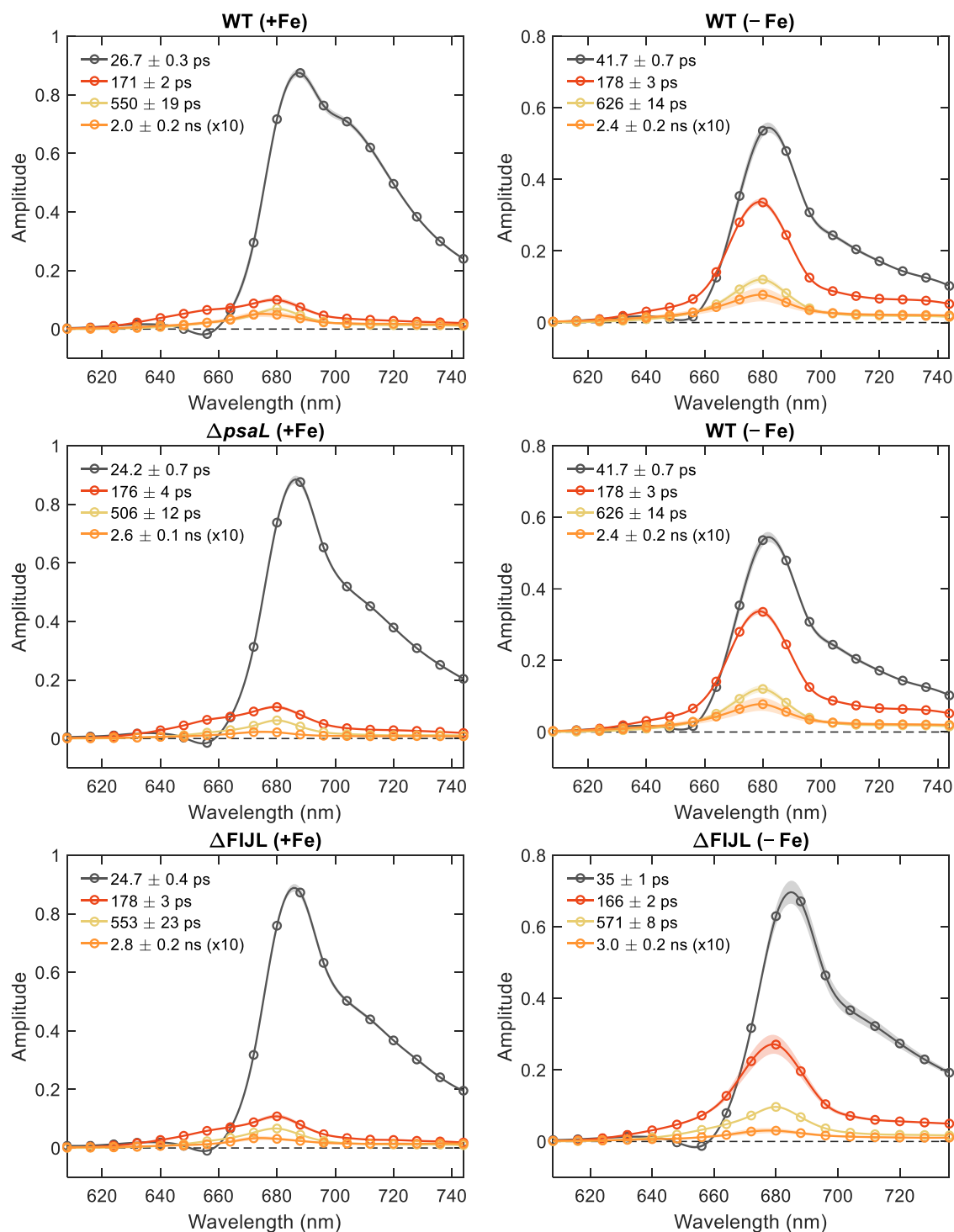


**Figure 5.** Decay-associated emission spectra (DAES) of intact *S. 6803* cells (WT,  $\Delta psaL$  and  $\Delta FIJL$  mutants) grown in regular BG-11 medium (+Fe) and in a medium devoid of iron (-Fe), obtained by global lifetime analysis of the fluorescence decays recorded at room temperature with 440 nm excitation. The DAES are scaled so that their sum is equal to one at 680 nm. The spectra are averages of 7 to 11 independent replicates. The final DAES (2 to 3 ns) is magnified by a factor of 10. The shaded areas represent SE.

fluorescence spectroscopy at 77 K performed on this super-complex showed an IsiA–PSI energy transfer component with a lifetime of 55 ps—which is comparable to the lifetimes determined here for whole cells. The authors also observed a 120 ps decay lifetime at 707 nm, which was attributed mainly

to excitation quenching. We cannot rule out the existence of such a component in the present system, as it would be mixed with the PSI decay components; however, it is worth emphasizing that the 80 to 90 ps DAES of cells with either trimeric or monomeric PSI clearly shows the occurrence of

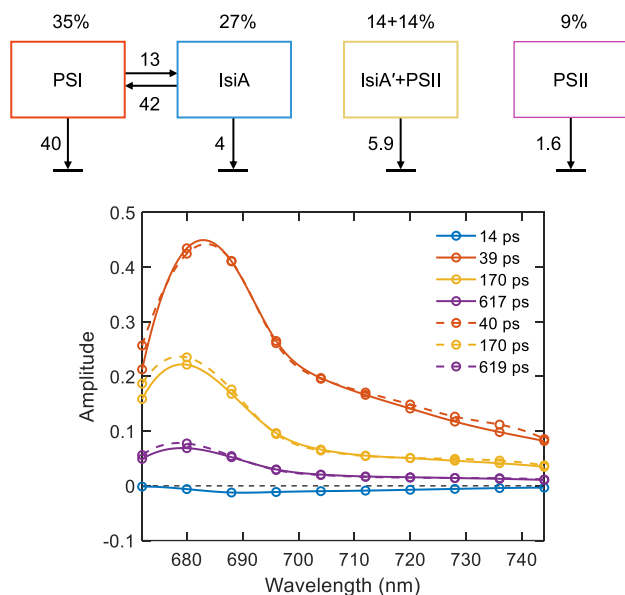


**Figure 6.** Kinetic model of PSI–IsiA fluorescence in *S. 6803*  $\Delta psal$  cells. The 4 compartments represent PSI–IsiA complexes, unconnected IsiA and PSii. The decay and energy transfer rate constants ( $\text{ns}^{-1}$ ) are indicated next to the arrows. The numbers above the compartments indicate the relative excitation of each compartment, proportional to the number of Chls. The PSI and IsiA emission spectra are modeled using the area-normalized DAES obtained from isolated complexes and PSii is represented by the PSii-associated DAES (500 ps) of iron-replete cells. The graphs show the model DAES (solid lines), compared with the DAES obtained from global lifetime analysis of the measured fluorescence kinetics of  $\Delta psal$  cells.

IsiA–PSi energy transfer on this timescale. Apart from these subtle differences that could well be species-dependent, there is a marked similarity in the functional architecture of PSI–IsiA in the 2 cyanobacterial species regardless of the oligomeric state of PSI.

The structural robustness of the PSI–IsiA supercomplex observed *in vitro* (Chauhan et al. 2011) is the basis for resilient energy transfer. From these results, it can be assumed that the primary physiological role of IsiA is light harvesting. However, the time-resolved fluorescence data (at 77 K and room temperature) suggest that a sizeable population of IsiA (approximately 40% of the total IsiA) is not functionally coupled to PSI. These results support electron microscopy studies on iron-stressed cyanobacteria that have found the presence of IsiA aggregates unconnected to PSI in cells (Yeremenko et al. 2004). The iron-stressed cells have significantly increased emission at 680 nm on an equal Chl basis (Table 1), similar to the results of Schrader et al. (2011) with *S. 6803* grown in iron-deficient nutrient-rich media. The increase in fluorescence was attributed to the existence of IsiA aggregates that are not connected to reaction centers.

### Dual role of IsiA

In line with previous studies, we show that under iron stress, cells can accumulate IsiA in excess of what is needed for

**Table 2.** Quantification of IsiA based on time-resolved fluorescence

Strain	PSi (% Chl)	IsiA (% Chl)	Free IsiA (% Chl)	PSii (% Chl)	IsiA:PSi (mol:mol)	Free IsiA:PSi (mol:mol)
WT	26	32	21	21	6.8	4.5
$\Delta psal$	35	27	15	22	4.2	2.3
$\Delta FIJL$	45	24	13	18	2.8	1.5

functional light harvesting by PSI, which serves a dual function. It has been seen by electron microscopy that IsiA builds supercomplexes without PSI under prolonged iron stress (Yeremenko et al. 2004). We observe both IsiA connected to PSI and unbound IsiA aggregates in a ratio of approximately 1.5:1 in WT *S. 6803*. According to *in vitro* studies, unconnected IsiA aggregates provide protection for PSii from photooxidation (Yeremenko et al. 2004; Havaux et al. 2005; Ihalainen et al. 2005; van der Weij-de et al. 2007). Similar to LHCii in land plants, IsiA is suggested to play a dual role, increasing the absorption cross-section of PSI on the onset of iron stress and regulating and balancing the light-harvesting to protect PSii from overexcitation by shading (Yeremenko et al. 2004; van der Weij-de et al. 2007). The substantial size of the unconnected IsiA pool (~40% of the total IsiA) appears to support such a role.

### The accumulation of IsiA depends on the PSi architecture

The functional importance of the trimeric organization of PSi in cyanobacteria has been puzzling. Recently, it was shown that the oligomeric state has an effect on the abundance and architecture of PBS and the distribution of excitation energy harvested by PBSs between PSii and PSi (Akhtar et al. 2022). The 2 mutant strains of *S. 6803* with monomeric PSi— $\Delta psal$  and  $\Delta FIJL$  had lower phycocyanin content, and their PBS delivered less excitation energy to PSi, indicating that the trimeric PSi organization facilitates PBS–PSi energy transfer. In this study, we subjected those mutant strains of *S. 6803* to iron-limiting conditions to investigate how the PSi architecture and subunit composition affect the accumulation of IsiA and the IsiA:PSi energy transfer.

All experimental approaches—steady-state and time-resolved fluorescence, CD spectroscopy and immunoblotting—show that the monomeric PSi mutants have significantly reduced IsiA content compared with the WT. All analyses show that the IsiA content decreases in the order WT >  $\Delta psal$  >  $\Delta FIJL$ . Therefore, the accumulation of IsiA in iron-stressed cells depends not only on the presence of the PsaL subunit but also on the PsaF/PsaJ subunits. Kouřil et al. (2003) showed that the PSI–IsiA supercomplexes are smaller in the absence of PsaF/PsaJ subunits and proposed that these subunits are needed for the binding of IsiA to PSi. In agreement with the microscopy studies, we find that PSi in the  $\Delta FIJL$  mutant binds less than half the number of IsiA complexes than WT PSi. We conclude that the accumulation of IsiA in the thylakoid membrane is controlled by

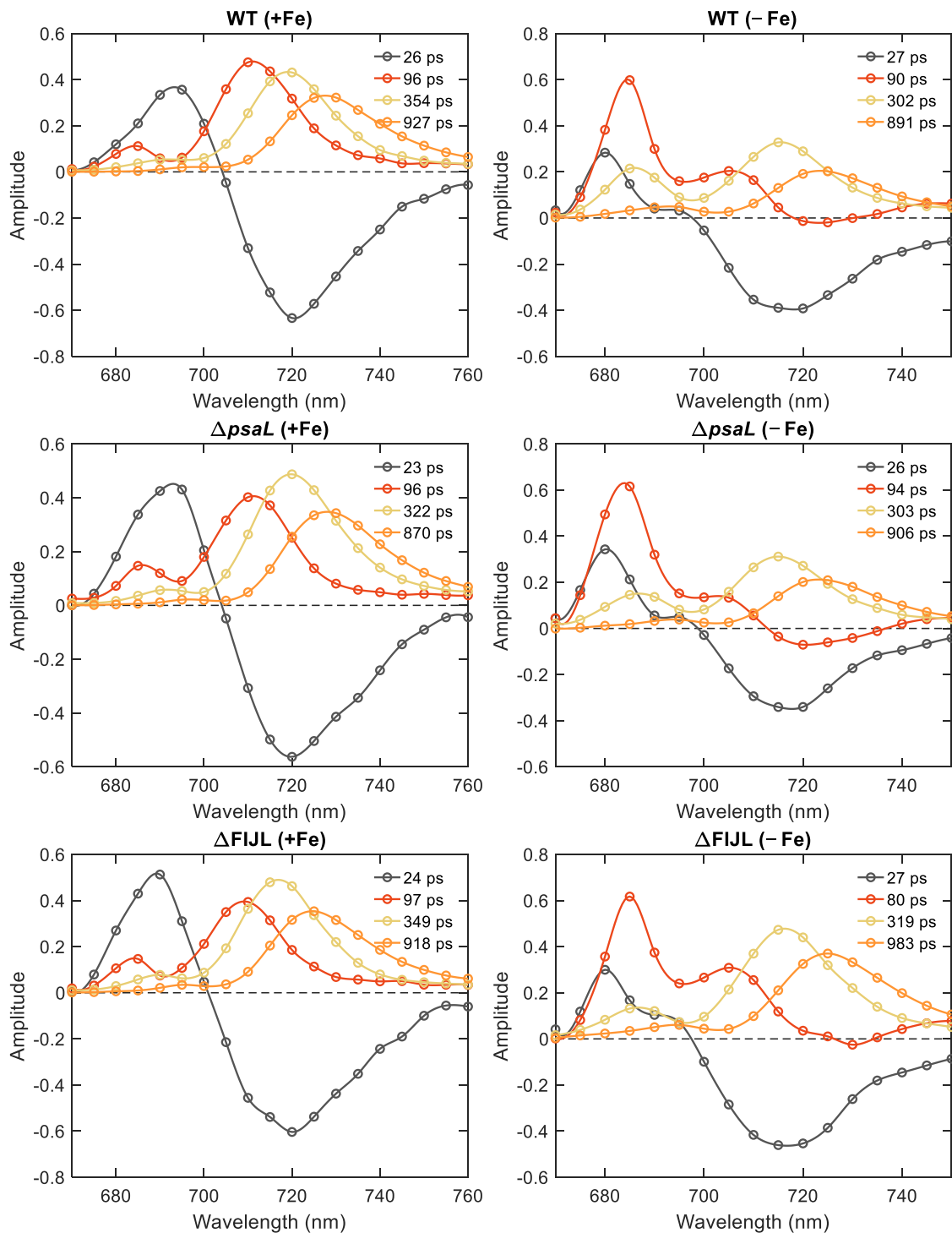


**Figure 7.** DAES of *S. 6803* cells (WT,  $\Delta psal$ , and  $\Delta FIJL$  mutants) grown in regular BG-11 medium (+Fe) and in a medium devoid of iron (–Fe), obtained by global lifetime analysis of the fluorescence decays recorded at 77 K with 440 nm excitation. The DAES amplitudes are scaled, so that their sum at the maximum is 1.

its ability to functionally connect to the PSI trimers; however, the exact feedback mechanism that regulates the expression of *IsiA* remains to be elucidated.

It could be expected that if *IsiA* does not form stable PSI–*IsiA* supercomplexes with the mutant PSI, a larger fraction will remain unconnected to PSI in the mutant cells. This,

however, does not seem to be the case, as the mutants have equally reduced pools of connected and unconnected *IsiA* compared with the WT *S. 6803* strain and approximately equal ratios of connected/free *IsiA* (Table 2). According to the microscopically determined structures of PSI–*IsiA*, each protomer should bind 6 *IsiA* subunits (Nagao et al. 2021). If we

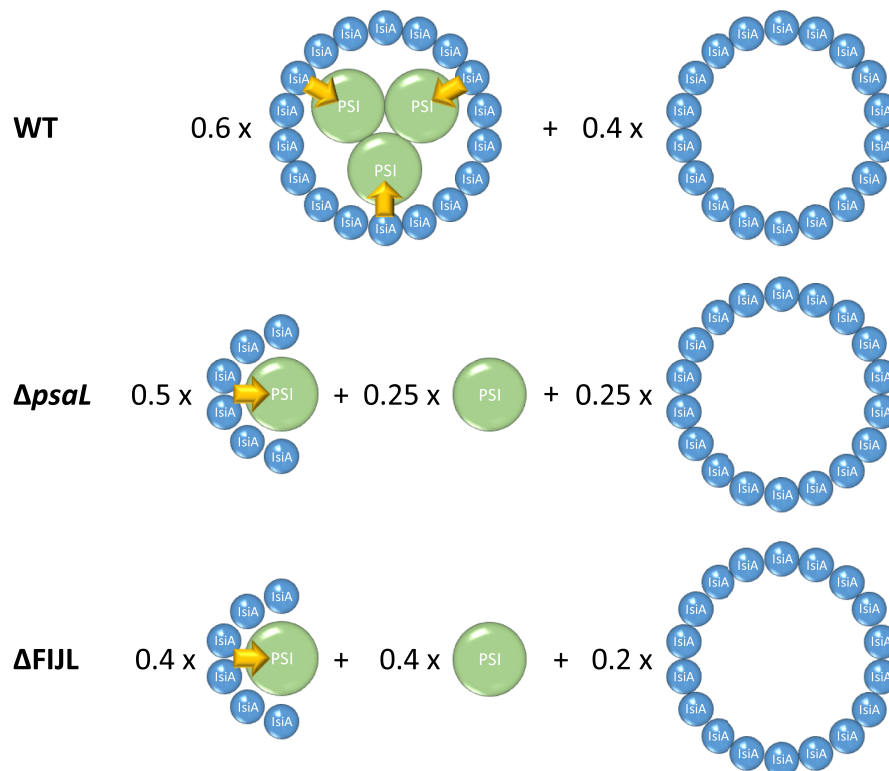


**Figure 8.** Schematic illustration of the IsiA, PSI, and PSI–IsiA content in *S. 6803* cells—wild type (WT), and the mutants lacking PSI subunits L and I ( $\Delta psal$ ) and F, I, J, L ( $\Delta FIJL$ ). The molar coefficients of the different types of supercomplexes are estimated based on Table 2, with the assumption that the majority of PSI–IsiA complexes bind 6 IsiA subunits per PSI monomer. The arrows indicate the existence of IsiA–PSI energy transfer.

take this ratio as representative of the majority of the supercomplexes in our experimental conditions, then the average IsiA:PSI stoichiometry suggests that a third of the PSI complexes in  $\Delta psal$  and one-half in  $\Delta FIJL$  bind no IsiA. This is illustrated schematically in Fig. 8. We can speculate that in the strains with subunit-depleted PSI, IsiA cannot sufficiently enhance the PSI absorption cross-section, and consequently, the cells maintain higher relative PSI content. More experiments are needed to test whether the altered acclimation strategy in the mutants will substantially hamper their capacity to grow under prolonged iron limitation conditions.

## Conclusions

To summarize, this study shows that IsiA formed functional supercomplexes in iron-stressed cells where energy was efficiently transferred to PSI in a manner similar to isolated PSI–IsiA complexes. Subunit-depleted PSI was unable to accommodate the same number of IsiA as the trimeric WT PSI, resulting in a smaller effective cross-section and leading to an overall lower IsiA content and higher PSI content on a Chl basis. These results strongly support the light-harvesting role of IsiA *in vivo*, as well as the role of the PsaF/PsaJ subunits, in mediating PSI–IsiA interaction. At the same time, the observation of large fractions of IsiA that are not functionally connected to PSI in all 3 *S. 6803* strains suggests that light harvesting is not the only functional role of the complex under iron limitation conditions.

Since both mutants with monomeric PSI displayed substantially reduced ability to functionally bind IsiA, this study represents further evidence for a specific physiological role of the oligomerization of PSI in cyanobacteria, in addition to the recently demonstrated role of trimeric PSI in facilitating energy transfer from PBS (Akhtar et al. 2022).

The findings shed light on IsiA's dual function in light harvesting and photoprotection in cyanobacteria under iron stress conditions. The results also demonstrate the possibility for quantitative spectroscopic detection of IsiA and its functional state in live cyanobacterial cells, which could be utilized to develop specific biosensors for assessing iron bioavailability and iron limitation stress in the field (Schrader Milligan and Behrenfeld 2011). Further research can explore the specific mechanisms and regulatory factors involved in the formation of PSI–IsiA supercomplexes and the dynamics of IsiA aggregation, contributing to a deeper understanding of the complex interplay between light harvesting and photoprotection in photosynthetic organisms.

## Materials and methods

### Growth conditions and preparation

*Synechocystis* sp. PCC 6803 (*S. 6803*) cells were grown photoautotrophically in BG-11 medium under continuous white fluorescent light ( $\sim 35 \mu\text{mol photons m}^{-2} \text{s}^{-1}$ ) at 30 °C. The WT strain (culturable under light-activated heterotrophic

growth and maintained in our lab), the  $\Delta psal$  mutant, obtained in the same WT background (Kłodawska et al. 2015), and the subunit-depleted  $\Delta FIJL$  mutant (Malavath et al. 2018) were used in this study. Iron-stressed cultures were obtained by inoculating the cells in BG-11 medium lacking iron-containing compounds. The cultures were grown for 1 wk. Thylakoid membranes were prepared as described in Akhtar et al. (2021). PSI–IsiA and IsiA complexes were isolated according to Yermenko et al. (2004) with small modifications. The thylakoid membranes were solubilized by incubating with 1% *n*-dodecyl- $\beta$ -maltoside ( $\beta$ -DDM) on ice. The unsolubilized material was removed by centrifugation at 30,000 g for 30 min. The supernatant was filtered through 0.45  $\mu$ m filters and loaded on an ion-exchange chromatography column (Hi-Trap Capto Q ImpRes, Cytiva, USA). The fractions containing PSI–IsiA were eluted using a 0 to 300 mM  $Mg_2SO_4$  gradient, concentrated, and further purified using a size-exclusion chromatography column (HiPrep 16/60 Sephacryl S-300 HR, Cytiva, USA).

### Chl content determination

Chls were extracted from the cell suspensions in 90% methanol, and the Chl contents were determined spectrophotometrically using molar absorption coefficients described in Lichtenthaler (1987).

### Immunoblot analysis

Suspension of thylakoid membranes containing 1  $\mu$ g Chl was mixed with 6 $\times$  Laemmli buffer (375 mM Tris/HCl [pH 6.8], 60% [v/v] glycerin, 12.6% [w/v] sodium dodecyl sulfate, 600 mM dithiothreitol, 0.09% [w/v] bromophenol blue) and incubated at 75 °C for 10 min before loading. Proteins were fractionated on SDS-PAGE and immunoblotted with the corresponding polyclonal antibodies (produced in rabbits) purchased from Agrisera AB: IsiA (AS 06 111), 1:1000 and PsaA (AS 06 172), 1:2000. The SuperSignal West Pico PLUS Chemiluminescent Substrate (Thermo Scientific) was used to detect these proteins with horseradish peroxidase-conjugated, antirabbit secondary antibody (Bio-Rad #1706515).

### Absorption and CD spectroscopy

Absorption and CD spectra in the range of 350 to 750 nm were recorded at room temperature with an Evolution 500 dual-beam spectrophotometer (Thermo Fisher Scientific, USA) and a J-815 spectropolarimeter (Jasco, Japan), respectively. The measurements were performed in a standard glass cuvette of 1-cm optical path length with 1 nm spectral bandwidth. The absorption spectra of the cells were corrected for the baseline by using bleached cells as a reference. CD spectra in the UV region were measured at the B23 CD beamline of the Diamond synchrotron (UK). For synchrotron-radiation CD measurements, the samples were placed in 0.2 mm quartz cuvettes.

### Steady-state fluorescence spectroscopy

Fluorescence emission spectra in the visible range were measured at room temperature and 77 K using an FP-8500 (Jasco, Japan)

spectrofluorometer. The samples were diluted to absorbance of 0.1 per cm at the red maximum. Emission spectra in the range of 620 to 780 nm were recorded with excitation wavelengths of 440 and 580 nm and an excitation/emission bandwidth of 2.5 nm. The measurements were performed with 1 nm increment and 1 or 4 s integration time for room temperature and 77 K, respectively. For measurements at 77 K, samples were cooled in an optical cryostat (Optistat DN, Oxford Instruments, UK) or a home-built accessory filled with liquid nitrogen. The spectra are corrected for the spectral sensitivity of the instrument using a calibrated light source (ESC-842, Jasco) as a reference.

### Time-resolved fluorescence spectroscopy

Picosecond time-resolved fluorescence measurements were performed with a time-correlated single-photon counting instrument (FluoTime 200/PicoHarp 300 spectrometer, PicoQuant, Germany) equipped with a microchannel plate detector (R3809, Hamamatsu, Japan). Excitation was provided by a Fianium WhiteLase Micro (NKT Photonics, UK) supercontinuum laser, generating white-light pulses with a repetition rate of 20 MHz. An excitation wavelength of 440 nm was used to excite selectively Chls. The fluorescence decays were recorded at wavelengths of 608 to 744 nm with 8 nm steps at room temperature and 605 to 750 nm with 5 nm steps at 77 K. All the samples were diluted to an absorbance of 0.03 at the excitation wavelength. For the room temperature measurements, the suspension (whole cells or isolated thylakoids) was placed in a 1-mm flow cell and circulated at a flow rate of 4 mL/min. For 77 K measurements, the suspension was placed in a 1 mm demountable cryogenic quartz cell and cooled in an optical cryostat (Optistat DN, Oxford Instruments, UK). The total instrument response (IRF) measured using 1% Ludox as scattering solution has a width of 40 ps. The data are corrected for the spectral response of the detector. Global multiexponential lifetime analysis with IRF deconvolution was performed using MATLAB. Essentially, the time and wavelength-dependent fluorescence intensity  $F(t, \lambda)$  are described as:

$$F(t, \lambda) = \text{IRF}(t - \Delta t(\lambda)) \otimes \sum_i a_i(\lambda) \exp\left(-\frac{t}{\tau_i}\right)$$

where  $\tau_i$  and  $a_i(\lambda)$  are decay lifetimes and DAES, respectively. For comparison between datasets, the DAES amplitudes are scaled, so that their sum at the peak wavelength is equal to 1:

$$a_i(\lambda) = \frac{a_i(\lambda)}{\sum a_i(\lambda_{\max})}$$

### Statistical analysis

Whenever appropriate, data are presented as mean  $\pm$  SE, obtained from independent measurements on different cell batches. The statistical significance, or lack thereof, of differences between the 2 mutant strains and the WT is reported based on single-factor ANOVA ( $\alpha = 0.01$ ).

## Accession numbers

Sequence data from this article can be found in the GenBank/EMBL data libraries under accession numbers listed in [Supplemental Table S3](#).

## Acknowledgments

We thank Prof. Dario Leister for the gift of the  $\Delta$ FIJL mutant of *S. 6803*.

## Author contributions

P.A. and P.H.L. conceptualized the study; P.A. performed most experiments. F.B.-V. maintained cyanobacterial cultures, isolated thylakoid membranes, and participated in spectroscopic measurements. S.K. and S.Z.T. designed and performed the immunoblotting study. All authors have contributed to the writing of the manuscript and given approval to the final version.

## Supplemental data

The following materials are available in the online version of this article.

**Supplemental Figure S1.** Absorption spectra of *Synechocystis* sp. PCC 6803 WT,  $\Delta$ psaL, and  $\Delta$ FIJL cells grown for 7 d in control BG11 medium (+Fe) or in a medium without iron (−Fe).

**Supplemental Figure S2.** Fluorescence emission spectra of intact cells at 77 K with 580 nm excitation light.

**Supplemental Figure S3.** Fluorescence emission spectra of isolated thylakoid membranes at 77 K with 440 nm excitation light.

**Supplemental Figure S4.** Room temperature CD spectra of IsiA and PSI–IsiA complexes in the UV region.

**Supplemental Figure S5.** DAES of PSI isolated from *Synechocystis* sp. PCC 6803 WT cells grown in normal BG11 medium.

**Supplemental Figure S6.** DAES of thylakoid membranes isolated from *Synechocystis* cells obtained by global lifetime analysis of the fluorescence decays recorded at room temperature with 440 nm excitation.

**Supplemental Figure S7.** Comparison of steady-state fluorescence emission spectra of iron-stressed *Synechocystis* WT cells, isolated IsiA, and PSI–IsiA complexes, recorded at room temperature with 440 nm excitation.

**Supplemental Figure S8.** Kinetic model of PSI–IsiA fluorescence in *Synechocystis* WT and  $\Delta$ FIJL cells.

**Supplemental Table S1.** Peak analysis of the 77 K emission spectra of thylakoid membranes.

**Supplemental Table S2.** Relative area of the room temperature DAES of iron-stressed cells.

**Supplemental Table S3.** Gene/protein accession numbers.

**Supplemental Method S1.** Quantification of IsiA from time-resolved fluorescence.

## Funding

The work was supported by grants from the National Research, Development and Innovation Office (NKFI FK-139067 to P.A. and ANN-144012 and 2018-1.2.1-NKP-2018-00009 to P.H.L.) and the Hungarian Research Network (SA-76/2021 to P.A.). CD measurements at the B23 beamline of the Diamond Light Source Ltd. were supported by the project CALIPSOplus under Grant Agreement 730872 from the EU Framework Program for Research and Innovation HORIZON 2020.

*Conflict of interest statement.* None declared.

## Data availability

The data underlying this article will be shared on reasonable request to the corresponding authors.

## References

- Akhtar P, Biswas A, Balog-Vig F, Domonkos I, Kovács L, Lambrev PH.** Trimeric photosystem I facilitates energy transfer from phycobilisomes in *Synechocystis* sp. PCC 6803. *Plant Physiol.* 2022;**189**(2): 827–838. <https://doi.org/10.1093/plphys/kiac130>
- Akhtar P, Biswas A, Kovacs L, Nelson N, Lambrev PH.** Excitation energy transfer kinetics of trimeric, monomeric and subunit-depleted Photosystem I from *Synechocystis* PCC 6803. *Biochem J.* 2021;**478**(7):1333–1346. <https://doi.org/10.1042/BCJ20210021>
- Akhtar P, Biswas A, Petrova N, Zakar T, van Stokkum IHM, Lambrev PH.** Time-resolved fluorescence study of excitation energy transfer in the cyanobacterium *Anabaena* PCC 7120. *Photosynth Res.* 2020;**144**(2):247–259. <https://doi.org/10.1007/s11120-020-00719-w>
- Akita F, Nagao R, Kato K, Nakajima Y, Yokono M, Ueno Y, Suzuki T, Dohmae N, Shen J-R, Akimoto S, et al.** Structure of a cyanobacterial photosystem I surrounded by octadecameric IsiA antenna proteins. *Commun Biol.* 2020;**3**(1):232. <https://doi.org/10.1038/s42003-020-0949-6>
- Andrizhiyevskaya EG, Frolov D, van Grondelle R, Dekker JP.** Energy transfer and trapping in the photosystem I complex of *Synechococcus* PCC 7942 and in its supercomplex with IsiA. *Biochim Biophys Acta.* 2004;**1656**(2–3):104–113. <https://doi.org/10.1016/j.bbabi.2004.02.002>
- Andrizhiyevskaya EG, Schwabe TME, Germano M, D'Haene S, Kruij J, van Grondelle R, Dekker JP.** Spectroscopic properties of PSI–IsiA supercomplexes from the cyanobacterium *Synechococcus* PCC 7942. *Biochim Biophys Acta.* 2002;**1556**(2–3):265–272. [https://doi.org/10.1016/S0005-2728\(02\)00371-7](https://doi.org/10.1016/S0005-2728(02)00371-7)
- Bibby TS, Nield J, Barber J.** Iron deficiency induces the formation of an antenna ring around trimeric photosystem I in cyanobacteria. *Nature.* 2001a;**412**(6848):743–745. <https://doi.org/10.1038/35089098>
- Bibby TS, Nield J, Barber J.** Three-dimensional model and characterization of the iron stress-induced CP43'–photosystem I supercomplex isolated from the cyanobacterium *Synechocystis* PCC 6803. *J Biol Chem.* 2001b;**276**(46):43246–43252. <https://doi.org/10.1074/jbc.M106541200>
- Blankenship RE.** Molecular mechanisms of photosynthesis. 3rd ed. Hoboken (NJ): Wiley; 2021.
- Boekema E, Hifney A, Yakushevska A, Piotrowski M, Keegstra W, Berry S, Michel K-P, Pistorius E, Kruij J.** A giant chlorophyll–protein complex induced by iron deficiency in cyanobacteria. *Nature.* 2001;**412**(6848):745–748. <https://doi.org/10.1038/35089104>
- Burnap RL, Troyan T, Sherman LA.** The highly abundant chlorophyll–protein complex of iron-deficient *Synechococcus* sp. PCC7942 (CP43') is encoded by the isiA gene. *Plant Physiol.* 1993;**103**(3): 893–902. <https://doi.org/10.1104/pp.103.3.893>

- Chauhan D, Folea IM, Jolley CC, Kouřil R, Lubner CE, Lin S, Kolber D, Wolfe-Simon F, Golbeck JH, Boekema EJ.** A novel photosynthetic strategy for adaptation to low-iron aquatic environments. *Biochemistry*. 2011;**50**(5):686–692. <https://doi.org/10.1021/bi1009425>
- Chen H-Y, Bandyopadhyay A, Pakrasi H.** Function, regulation and distribution of IsiA, a membrane-bound chlorophyll a-antenna protein in cyanobacteria. *Photosynthetica*. 2018;**56**(SPECIAL ISSUE):322–333. <https://doi.org/10.1007/s11099-018-0787-7>
- Chen H-YS, Liberton M, Pakrasi HB, Niedzwiedzki DM.** Reevaluating the mechanism of excitation energy regulation in iron-starved cyanobacteria. *Biochim Biophys Acta Bioenerg*. 2017;**1858**(3):249–258. <https://doi.org/10.1016/j.bbabi.2017.01.001>
- Fraser JM, Tulk SE, Jeans JA, Campbell DA, Bibby TS, Cockshutt AM.** Photophysiological and photosynthetic complex changes during iron starvation in *Synechocystis* sp. PCC 6803 and *Synechococcus elongatus* PCC 7942. *PLoS One*. 2013;**8**(3):e59861. <https://doi.org/10.1371/journal.pone.0059861>
- Fromme P, Melkozernov A, Jordan P, Krauss N.** Structure and function of photosystem I: interaction with its soluble electron carriers and external antenna systems. *FEBS Lett*. 2003;**555**(1):40–44. [https://doi.org/10.1016/S0014-5793\(03\)01124-4](https://doi.org/10.1016/S0014-5793(03)01124-4)
- Gobets B, van Grondelle R.** Energy transfer and trapping in photosystem I. *Biochim Biophys Acta*. 2001;**1507**(1–3):80–99. [https://doi.org/10.1016/S0005-2728\(01\)00203-1](https://doi.org/10.1016/S0005-2728(01)00203-1)
- Guikema JA, Sherman LA.** Organization and function of chlorophyll in membranes of cyanobacteria during iron starvation. *Plant Physiol*. 1983;**73**(2):250–256. <https://doi.org/10.1104/pp.73.2.250>
- Havaux M, Guedeney G, Hagemann M, Yeremenko N, Matthijs HC, Jeanjean R.** The chlorophyll-binding protein IsiA is inducible by high light and protects the cyanobacterium *Synechocystis* PCC6803 from photooxidative stress. *FEBS Lett*. 2005;**579**(11):2289–2293. <https://doi.org/10.1016/j.febslet.2005.03.021>
- Ihalainen JA, D'Haene S, Yeremenko N, van Roon H, Arteni AA, Boekema EJ, van Grondelle R, Matthijs HC, Dekker JP.** Aggregates of the chlorophyll-binding protein IsiA (CP43') dissipate energy in cyanobacteria. *Biochemistry*. 2005;**44**(32):10846–10853. <https://doi.org/10.1021/bi0510680>
- Jia A, Zheng Y, Chen H, Wang Q.** Regulation and functional complexity of the chlorophyll-binding protein IsiA. *Front Microbiol*. 2021;**12**:774107. <https://doi.org/10.3389/fmicb.2021.774107>
- Keren N, Aurora R, Pakrasi HB.** Critical roles of bacterioferritins in iron storage and proliferation of Cyanobacteria. *Plant Physiol*. 2004;**135**(3):1666–1673. <https://doi.org/10.1104/pp.104.042770>
- Kłodawska K, Kovács L, Várkonyi Z, Kis M, Sozer Ö, Laczko-Dobos H, Kóbori O, Domonkos I, Strzałka K, Gombos Z, et al.** Elevated growth temperature can enhance photosystem I trimer formation and affects xanthophyll biosynthesis in cyanobacterium *Synechocystis* sp. PCC6803 cells. *Plant Cell Physiol*. 2015;**56**(3):558–571. <https://doi.org/10.1093/pcp/pcu199>
- Kojima K, Suzuki-Maenaka T, Kikuchi T, Nakamoto H.** Roles of the cyanobacterial isiABC operon in protection from oxidative and heat stresses. *Physiol Plantarum*. 2006;**128**(3):507–519. <https://doi.org/10.1111/j.1399-3054.2006.00781.x>
- Kouřil R, Arteni AA, Lax J, Yeremenko N, D'Haene S, Rögner M, Matthijs HC, Dekker JP, Boekema EJ.** Structure and functional role of supercomplexes of IsiA and Photosystem I in cyanobacterial photosynthesis. *FEBS Lett*. 2005;**579**(15):3253–3257. <https://doi.org/10.1016/j.febslet.2005.03.051>
- Kouřil R, Yeremenko N, D'Haene S, Yakushevskaya AE, Keegstra W, Matthijs HC, Dekker JP, Boekema EJ.** Photosystem I trimers from *Synechocystis* PCC 6803 lacking the Psaf and PsaJ subunits bind an IsiA ring of 17 units. *Biochim Biophys Acta Bioenerg*. 2003;**1607**(1):1–4. <https://doi.org/10.1016/j.bbabi.2003.08.002>
- Lichtenthaler HK.** Chlorophylls and carotenoids: pigments of photosynthetic biomembranes. *Methods Enzymol*. 1987;**148**:350–382. [https://doi.org/10.1016/0076-6879\(87\)48036-1](https://doi.org/10.1016/0076-6879(87)48036-1)
- Malavath T, Caspy I, Netzer-El SY, Klaiman D, Nelson N.** Structure and function of wild-type and subunit-depleted photosystem I in *Synechocystis*. *Biochim Biophys Acta Bioenerg*. 2018;**1859**(9):645–654. <https://doi.org/10.1016/j.bbabi.2018.02.002>
- Melkozernov AN, Bibby TS, Lin S, Barber J, Blankenship RE.** Time-resolved absorption and emission show that the CP43 'antenna ring of iron-stressed *Synechocystis* sp. PCC6803 is efficiently coupled to the photosystem I reaction center core. *Biochemistry*. 2003;**42**(13):3893–3903. <https://doi.org/10.1021/bi026987u>
- Nagao R, Kato K, Hamaguchi T, Ueno Y, Tsuboshita N, Shimizu S, Furutani M, Ehira S, Nakajima Y, Kawakami K.** Structure of a monomeric photosystem I core associated with iron-stress-induced-A proteins from *Anabaena* sp. PCC 7120. *Nat Commun*. 2023;**14**(1):920. <https://doi.org/10.1038/s41467-023-36504-1>
- Nagao R, Yokono M, Ueno Y, Suzuki T, Kato K, Kato K-H, Tsuboshita N, Jiang T-Y, Dohmae N, Shen J-R, et al.** Molecular organizations and function of iron-stress-induced-A protein family in *Anabaena* sp. PCC 7120. *Biochim Biophys Acta Bioenerg*. 2021;**1862**(1):148327. <https://doi.org/10.1016/j.bbabi.2020.148327>
- Öquist G.** Light-induced changes in pigment composition of photosynthetic lamellae and cell-free extracts from the blue-green alga *Anacystis nidulans*. *Physiol Plantarum*. 1974;**30**(1):45–48. <https://doi.org/10.1111/j.1399-3054.1974.tb04989.x>
- Park Yi, Sandström S, Gustafsson P, Öquist G.** Expression of the isiA gene is essential for the survival of the cyanobacterium *Synechococcus* sp. PCC 7942 by protecting photosystem II from excess light under iron limitation. *Mol Microbiol*. 1999;**32**(1):123–129. <https://doi.org/10.1046/j.1365-2958.1999.01332.x>
- Ryan-Keogh TJ, Macey AI, Cockshutt AM, Moore CM, Bibby TS.** The cyanobacterial chlorophyll-binding-protein isiA acts to increase the in vivo effective absorption cross-section of psi under iron limitation. *J Phycol*. 2012;**48**(1):145–154. <https://doi.org/10.1111/j.1529-8817.2011.01092.x>
- Schoffman H, Keren N.** Function of the IsiA pigment-protein complex in vivo. *Photosynth Res*. 2019;**141**(3):343–353. <https://doi.org/10.1007/s11120-019-00638-5>
- Schrader PS, Milligan AJ, Behrenfeld MJ.** Surplus photosynthetic antennae complexes underlie diagnostics of iron limitation in a cyanobacterium. *PLoS One*. 2011;**6**(4):e18753. <https://doi.org/10.1371/journal.pone.0018753>
- Singh AK, Li H, Sherman LA.** Microarray analysis and redox control of gene expression in the cyanobacterium *Synechocystis* sp. PCC 6803. *Physiol Plant*. 2004;**120**(1):27–35. <https://doi.org/10.1111/j.0031-9317.2004.0232.x>
- Singh AK, Sherman LA.** Reflections on the function of IsiA, a cyanobacterial stress-inducible, Chl-binding protein. *Photosynth Res*. 2007;**93**(1–3):17–25. <https://doi.org/10.1007/s11120-007-9151-7>
- Tian L, Gwizdala M, van Stokkum IH, Koehorst RB, Kirilovsky D, van Amerongen H.** Picosecond kinetics of light harvesting and photoprotective quenching in wild-type and mutant phycobilisomes isolated from the cyanobacterium *Synechocystis* PCC 6803. *Biophys J*. 2012;**102**(7):1692–1700. <https://doi.org/10.1016/j.bpj.2012.03.008>
- Toporik H, Li J, Williams D, Chiu P-L, Mazor Y.** The structure of the stress-induced photosystem I–IsiA antenna supercomplex. *Nat Struct Mol Biol*. 2019;**26**(6):443–449. <https://doi.org/10.1038/s41594-019-0228-8>
- van der Weij-de CD, Ihalainen JA, van de Vijver E, D'Haene S, Matthijs HC, van Grondelle R, Dekker JP.** Fluorescence quenching of IsiA in early stage of iron deficiency and at cryogenic temperatures. *Biochim Biophys Acta Bioenerg*. 2007;**1767**(12):1393–1400. <https://doi.org/10.1016/j.bbabi.2007.10.001>
- Vinnemeier J, Kunert A, Hagemann M.** Transcriptional analysis of the isiAB operon in salt-stressed cells of the cyanobacterium *Synechocystis* sp. PCC 6803. *FEMS Microbiol Lett*. 1998;**169**(2):323–330. <https://doi.org/10.1111/j.1574-6968.1998.tb13336.x>
- Yeremenko N, Kouřil R, Ihalainen JA, D'Haene S, van Oosterwijk N, Andrizhivetskaya EG, Keegstra W, Dekker HL, Hagemann M, Boekema EJ.** Supramolecular organization and dual function of the IsiA chlorophyll-binding protein in cyanobacteria. *Biochemistry*. 2004;**43**(32):10308–10313. <https://doi.org/10.1021/bi048772l>